IOP Publishing Journal of Optics
J. Opt. **16** (2014) 025401 (8pp) doi:10.1088/2040-8978/16/2/025401

Image hiding in time-averaged deformable moiré gratings

R Palivonaite[1], A Aleksa[1], A Paunksnis[2], A Gelzinis[2] and M Ragulskis[1]

[1] Research Group for Mathematical and Numerical Analysis of Dynamical Systems, Kaunas University of Technology, Studentu 50-222, Kaunas LT-51368, Lithuania
[2] Department of Ophthalmology, Lithuanian University of Health Sciences, Eiveniu 2, Kaunas LT-50009, Lithuania

E-mail: rita.palivonaite@ktu.lt, algiment.aleksa@ktu.lt, apaun@medi.lt, arvydas_gelzinis@yahoo.com and minvydas.ragulskis@ktu.lt

Received 17 September 2013, revised 13 November 2013
Accepted for publication 2 December 2013
Published 15 January 2014

Abstract
A new image hiding technique based on time-averaged moiré fringes is proposed in this paper. The secret image is embedded into a single cover image which is constructed as a deformable stochastic moiré grating. The secret image is leaked in the form of a time-averaged fringe when the cover image is deformed according to a predetermined periodic law of motion. The proposed image hiding approach opens new possibilities for the optical control of vibrating deformable structures.

Keywords: visual cryptography, geometric moiré, time-averaged fringe, Bessel functions
PACS numbers: 42.30.Ms, 46.40.-f, 07.10.-h

1. Introduction

Geometric moiré (GM) [1, 2] is a classical in-plane whole-field non-destructive optical experimental technique based on the analysis of visual patterns produced by the superposition of two regular gratings that geometrically interfere. A typical moiré grating is an array of alternately opaque and transparent equally spaced straight lines, but experimental applications exploiting concentric circles, cross-gratings, regular arrays of dots or even randomly distributed dots can be found in the engineering literature [3, 4]. Two basic goals exist in moiré pattern research. The first is the analysis of experimentally produced moiré patterns in order to determine displacements (or strains) at the centerlines of moiré fringes. Another goal is moiré pattern synthesis, when the generation of a certain predefined moiré pattern is required. The synthesis process involves the production of two images such that the required moiré pattern emerges when those images are superimposed [1]. The conditions ensuring that a desired moiré pattern will be present in the superposition of two images are predetermined; however, they do not specify these two original images uniquely. Several criteria are proposed in [5, 6] to resolve that freedom in moiré pattern synthesis.

Visual cryptography (VC) is a cryptographic technique which allows visual information (pictures, text, etc) to be encrypted in such a way that the decryption can be performed by the human visual system, without the aid of computers. VC was pioneered by Naor and Shamir in 1994 [7]. They demonstrated a visual secret sharing scheme, where an image was broken up into a number of shares so that only someone with all shares could decrypt the image. Each share was printed on a separate transparency, and decryption was performed by overlaying the shares. When all shares were overlaid, the original image would appear.

The main difference between GM and VC is that a single share is cryptographically secure in the VC setting (which in general is not true for GM). In other words, an eavesdropper having a single VC share has no possibility (visual or computational) to detect the secret image. Since 1994, many advances in visual cryptography have been made. Visual cryptography for color images has been proposed in [8, 9]. Ideal contrast visual cryptography schemes have been introduced in [10]. A general multi-secret visual cryptography scheme is presented in [11]; incrementing visual cryptography is described in [12]. A new cheating prevention visual cryptography scheme is discussed in [13]. In contrast to VC, moiré pattern synthesis applications have not experienced

such extensive developments (due to problems associated with cryptographic security).

Time average geometric moiré (TAGM) is a dynamic alternative to static double exposure GM. The principles of TAGM were developed in 1979 [14]. A single moiré grating is used in TAGM. A nontransparent image of the grating is printed on the surface of an oscillating body and time averaging techniques are used to record time-averaged moiré fringes [15]. Two different aspects of TAGM should be mentioned here. A moiré grating can be printed on the surface of a non-deformable body which performs in-plane oscillations with respect to a reference coordinate system (a non-deformable grating). Alternatively, a moiré grating can be formed on the surface of a deformable body [16]. Oscillating surface deformations would result in instantaneously deformed gratings and would yield a pattern of moiré fringes in the time-averaged image.

On the other hand (in analogy to GM), TAGM can be exploited not only for the optical analysis of vibrating structures but also for the synthesis of a predefined pattern of time-averaged fringes. Such a type of image hiding technique, when the secret image leaks in a form of a time-averaged moiré fringe in an oscillating non-deformable cover image, was first presented in [17]. A stochastic moiré grating is used to embed the secret into a single cover image, and the secret can be visually decoded by the naked eye only when the amplitude of the harmonic oscillations corresponds to an accurately preselected value. The fact that the naked eye cannot interpret the secret from a static cover image makes this image hiding technique similar to VC. Special computational algorithms are required to encode the image, but the decoding is completely visual. The difference from VC is that only a single cover image is used and that it should be oscillated in order to leak the secret. Also, although the cover image is not cryptographically secure such fusion of TAGM and VC deserves the title of dynamic visual cryptography (DVC) [18]. Different measures have been exploited to increase the security of DVC. Triangular waveforms [19] have been used as additional security measures in the scheme. It is important to note that visual decoding of all these DVC schemes is based on a non-deformable moiré grating—the cover image is oscillated, but not deformed.

The main objective of this paper is to develop a theoretical foundation for dynamic visual cryptography based on deformable moiré gratings. The formation of the cover image, image hiding procedures in the background moiré grating, and optical relationships governing the formation of time-averaged moiré fringes are discussed in detail. In fact, this is the main objective of this paper, which is organized as follows. The theoretical background of the problem is discussed in section 2; the construction of a deformable moiré grating is presented in section 3; the DVC scheme based on deformable gratings is illustrated in section 4; concluding remarks are given in section 5.

2. Theoretical background

2.1. A non-deformable moiré grating with a constant pitch

Let us consider a one-dimensional harmonic moiré grating:

$$F(x) = \frac{1}{2} + \frac{1}{2}\cos\left(\frac{2\pi}{\lambda}x\right) \tag{1}$$

where λ is the pitch of the grating; 0 corresponds to the black color, 1 corresponds to the white color and all intermediate numerical values of $F(x)$ correspond to an appropriate grayscale level. In other words, (1) describes a periodic variation of grayscale levels on a surface. Let us assume that this moiré grating is painted on the surface of a one-dimensional non-deformable body. Also, let us assume that this body oscillates around the state of equilibrium (without being deformed) and the deflection from the state of equilibrium does not depend on x:

$$u(x,t) = u(t) = a\sin(\omega t + \varphi), \tag{2}$$

where ω is the cyclic frequency, φ is the phase and a is the amplitude of oscillation. The resultant time-averaged image reads [16]:

$$\begin{aligned}\bar{F}(x) &= \lim_{T\to\infty}\frac{1}{T}\int_0^T F\left(x - a\sin(\omega t + \varphi)\right)\mathrm{d}t \\ &= \frac{1}{2} + \frac{1}{2}\cos\left(\frac{2\pi}{\lambda}x\right)J_0\left(\frac{2\pi}{\lambda}a\right),\end{aligned} \tag{3}$$

where T is the exposure time; J_0 is the zeroth order Bessel function of the first kind. The original moiré grating is mapped into a time-averaged fringe ($\bar{F}(x) = \frac{1}{2}$) when J_0 becomes equal to zero. In other words, the explicit relationship among the pitch of the moiré grating λ, the amplitude of harmonic oscillations a and the consecutive number of the time-averaged moiré fringe k reads:

$$\frac{2\pi}{\lambda}a_k = r_k; \qquad k = 1, 2, \ldots \tag{4}$$

where r_k is the kth root of J_0; a_k is the discrete value of the amplitude which results in the kth time-averaged fringe in the time-averaged image.

2.2. A deformable moiré grating with a constant pitch

Now let us consider the same moiré grating (1) plotted on the surface of a one-dimensional deformable body. Let us assume that the left end of this linear deformable body is motionlessly fixed at $x = 0$ and the right end is free at $x = x_1$ in the state of equilibrium. Let us assume that the amplitude of harmonic oscillations is equal to Ax_1 at $x = x_1$. Now the deflection from the state of equilibrium does depend on x:

$$u(x,t) = Ax\sin(\omega t + \varphi); \qquad 0 \le x \le x_1. \tag{5}$$

The instantaneous shape of the deformed grating F_d reads:

$$F_\mathrm{d}(x + u(x,t)) = F(x). \tag{6}$$

It would be tempting to express F_d in the following explicit form:

$$F_\mathrm{d}(x,t) = F\left(x - u(x,t)\right) \tag{7}$$

but such a transition leads to a crude mathematical error [16]—such an explicit expression holds only if $u(x,t)$ does not depend on x. Otherwise (if one wishes to construct an explicit

form of F_d), it is necessary to express x in terms of z from the following equality:

$$x + u(x, t) = z. \tag{8}$$

Luckily, it is possible to solve (8) when (5) holds. Thus, the explicit instantaneous expression of F_d reads [16]:

$$F_d(x, t) = F\left(\frac{x}{1 + A\sin(\omega t + \varphi)}\right) = \frac{1}{2} + \frac{1}{2}\cos\left(\frac{2\pi}{\lambda\,(1 + A\sin(\omega t + \varphi))}x\right). \tag{9}$$

Now, the time-averaged image reads:

$$\bar{F}_d(x) = \lim_{T\to\infty}\frac{1}{T}\int_0^T F_d(x, t)\,dt = \frac{1}{2\pi}\int_0^{2\pi} F_d(x, t)\,dt. \tag{10}$$

Unfortunately, the definite integral in (10) cannot be expressed in a form comprising ordinary functions.

Direct interpretation of (10) is impossible due to the interplay of infinite functional series. A computational interpretation of $\bar{F}_d(x)$ is presented in [16] and suggests that the formation of time-averaged fringes induced by an oscillating deformable moiré grating is somewhat similar to (3) under the assumption that the amplitude a increases continuously with x. This fact can be illustrated using the following reasoning. Equation (9) yields:

$$F_d(x, t) = \frac{1}{2} + \frac{1}{2}\cos\left(\frac{2\pi}{\lambda}x - \frac{2\pi}{\lambda}A\sin(\omega t + \varphi)x + O(A^2)\right). \tag{11}$$

Let us assume that A is not large. Note that (9) is defined only at $0 \le A < 1$ (a singularity exists at $A = 1$). Then, neglecting higher order terms results in the following approximation of (11):

$$F_d(x, t) \approx \frac{1}{2} + \frac{1}{2}\cos\left(\frac{2\pi}{\lambda}x\right)\cos\left(\frac{2\pi}{\lambda}A\sin(\omega t + \varphi)x\right) + \frac{1}{2}\sin\left(\frac{2\pi}{\lambda}x\right)\sin\left(\frac{2\pi}{\lambda}A\sin(\omega t + \varphi)x\right). \tag{12}$$

It is easy to prove that

$$\int_0^{2\pi}\sin\left(\frac{2\pi}{\lambda}A\sin(\omega t + \varphi)x\right)dt = 0 \tag{13}$$

because the sine function is an odd function. Then,

$$\bar{F}_d(x) \approx \frac{1}{2} + \frac{1}{2}\cos\left(\frac{2\pi}{\lambda}x\right)\lim_{T\to\infty}\frac{1}{T} \times \int_0^T\cos\left(\frac{2\pi}{\lambda}A\sin(\omega t + \varphi)x\right)dt = \frac{1}{2} + \frac{1}{2}\cos\left(\frac{2\pi}{\lambda}x\right)J_0\left(\frac{2\pi}{\lambda}Ax\right). \tag{14}$$

Therefore, time-averaged moiré fringes induced by an oscillating deformable grating with a constant pitch form at such x where:

$$x = \frac{r_k\lambda}{2\pi A}; \qquad k = 1, 2, \ldots, \tag{15}$$

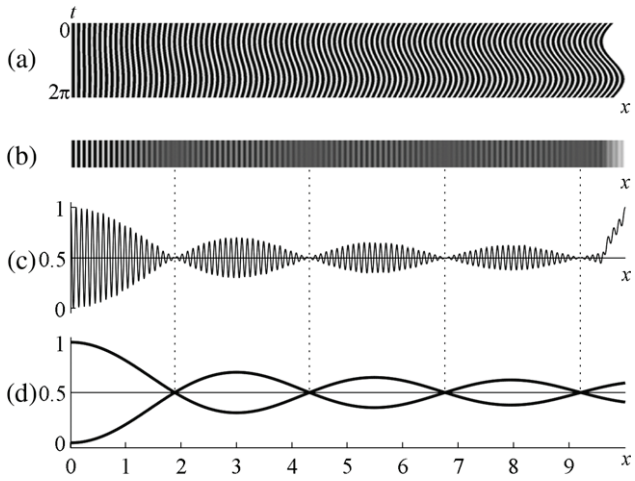

Figure 1. Geometric representation of time-averaged fringes induced by a deformable moiré grating with a constant pitch; $\lambda = 1$ mm; $A = 0.02$. The oscillation of the deformable one-dimensional moiré grating in time is illustrated in (a); the time-averaged image (in grayscale levels) is illustrated in (b); one-dimensional time-averaged grayscale levels are shown in (c); the envelope function $\bar{E}_d(x)$ is shown in (d).

and the envelope function $\bar{E}_d$ modulating the stationary grating can be approximated as:

$$\bar{E}_d(x) \approx \frac{1}{2} \pm \frac{1}{2}J_0\left(\frac{2\pi}{\lambda}Ax\right). \tag{16}$$

The oscillation of the deformable one-dimensional moiré grating in time is illustrated in figure 1(a); time-averaged grayscale levels are presented in figures 1(b) and (c); the envelope function is illustrated in figure 1(d). Note that the dimension of x in the x-axis of figure 1 (and all subsequent figures) is measured in centimeters (10 mm). The naked eye cannot perceive any approximation errors in (16).

3. A deformable moiré grating with a variable pitch

Dynamic visual cryptography is based on the formation of time-averaged moiré fringes in the areas occupied by the secret image in the encoded cover image (when the cover image is oscillated according to a predetermined law of motion) [17, 19]. In other words, the whole observation window comprising a constant pitch non-deformable moiré grating is transformed into a continuous time-averaged fringe. But that is not the case for a constant pitch deformable moiré grating (figure 1)—several localized time-averaged fringes may form in the observation window. This is completely unsatisfactory for dynamic visual cryptography.

The question is simple—is it possible to construct such a moiré grating as would be transformed into a continuous time-averaged fringe when the oscillations are governed by equation (5). An intuitive answer suggests a variable pitch deformable moiré grating—the amplitude of oscillation varies continuously from 0 at the left boundary of the one-dimensional structure up to the maximum at the right boundary of the observation window. From the mathematical point of view, the envelope function $\bar{E}_d$ should become equal

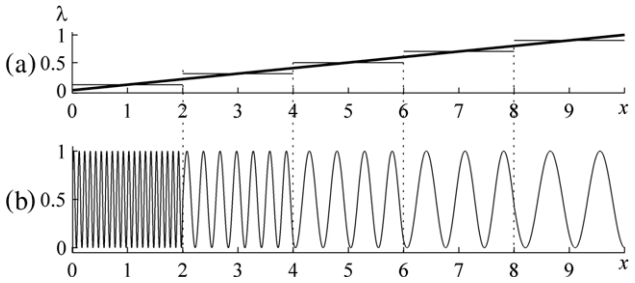

Figure 2. Formation of a moiré grating with a step-incremental pitch.

to 0.5 for all $0 \le x \le x_1$. That is possible if and only if $J_0\left(\frac{2\pi}{\lambda}Ax\right) = 0$. In other words, the pitch of the moiré grating must be a linear function of x:

$$\lambda = Lx, \tag{17}$$

where L can take one of the discrete values of L_k:

$$L_k = \frac{2\pi A}{r_k}; \qquad k = 1, 2, \ldots. \tag{18}$$

The assumption (17) is clear and natural—the higher is the amplitude of oscillations, the larger must be the pitch of the moiré grating. Unfortunately, such an assumption does not work—the deformable moiré grating (9) cannot be formed because the grating degenerates into a constant t:

$$F_{\mathrm{d}}(x,t) = \frac{1}{2} + \frac{1}{2}\cos\left(\frac{2\pi}{L\,(1 + A\sin(\omega t + \varphi))}\right). \tag{19}$$

In other words, the grayscale level on the surface of a deformable body oscillates as t varies but the grayscale level of the whole one-dimensional deformable body is constant at any instantaneous moment of time. This is no longer a model describing optical geometric moiré effects.

3.1. A deformable moiré grating with a step-incremental pitch

As shown previously, a continuous linear variation of the pitch of the moiré grating results in a degenerate optical model. Therefore, we construct a step-incremental pitch (figure 2) instead of assuming a continuous variation of the pitch. The number of finite-length intervals can be preselected at the beginning of the computational experiment but the pitch of the moiré grating is constant in the domain of every interval. Moreover, we employ a phase regularization algorithm [17] in order to avoid phase jumps at the boundary points between adjacent intervals (the reconstructed composite moiré grating is formed as a continuous function (figure 2(b))).

Such an approach for the formation of the moiré grating with a step-incremental pitch can be extended to a scheme where the length of the interval becomes equal to the distance between adjacent pixels. A schematic diagram illustrating the formation of such an 'extreme' moiré grating is presented in figure 3 by a thick gray curve. The size of the intervals on the x-axis corresponds to the size of a pixel; p_k corresponds to the kth pixel. First, equation (17) is used for the calculation

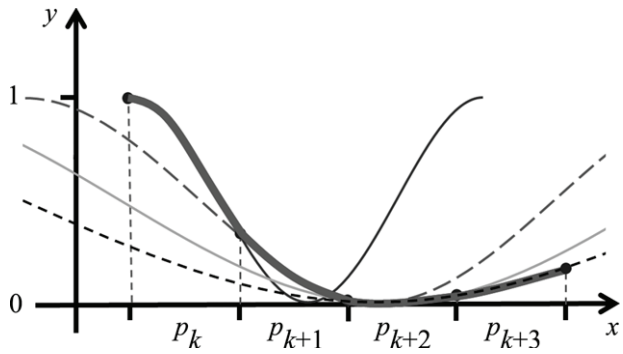

Figure 3. A schematic diagram illustrating the formation of a deformable moiré grating with a step-incremental pitch; p_k corresponds to the kth pixel. First, equation (17) is used for the calculation of the pitch of the moiré grating at the center of the kth pixel; the corresponding constant pitch grating is illustrated by a thin black line. The pitch of the moiré grating is then calculated at the center of the $(k+1)$th pixel; the corresponding constant pitch grating is illustrated by a gray dashed line. Note that the phase of the grating in the interval occupied by the $(k+1)$th pixel is set in such a way that the composite grating (denoted by the thick gray solid line) is a continuous function. The process is continued throughout the whole domain; the resulting composite moiré grating is illustrated by the thick gray solid line.

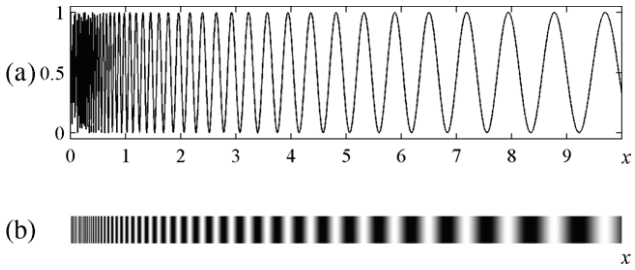

Figure 4. A variable pitch moiré grating (a) and its optical representation (b).

of the pitch of the moiré grating at the center of the kth pixel—the corresponding constant pitch grating is illustrated by a thin black line in figure 3. The pitch of the moiré grating is then calculated at the center of the $(k+1)$th pixel—the corresponding constant pitch grating is illustrated by a gray dashed line in figure 3. But the phase of the moiré grating in the zone occupied by the $(k+1)$th pixel is not arbitrary—it is selected in such a way that the composite grating is a continuous function (figure 3). The process is continued until the composite moiré grating is constructed in the whole domain $0 \le x \le x_1$—the reconstructed variable pitch moiré grating and its optical representation are shown in figure 4 (a) and (b). Note that the variable pitch deformable moiré grating does not degenerate into a constant—though equation (17) does hold true and $L = \frac{2\pi A}{r_1} = 0.1$. The singularity of the grating at $x = 0$ does not disappear—the resolution of the digital image in figure 4(a) is too low to reconstruct the fast variation of the grayscale level in the left side of the image.

In analogy to the computational experiment performed with the constant pitch deformable moiré grating (figure 1) we oscillate the variable pitch deformable moiré grating and reconstruct its time-averaged image (figure 5). The image in

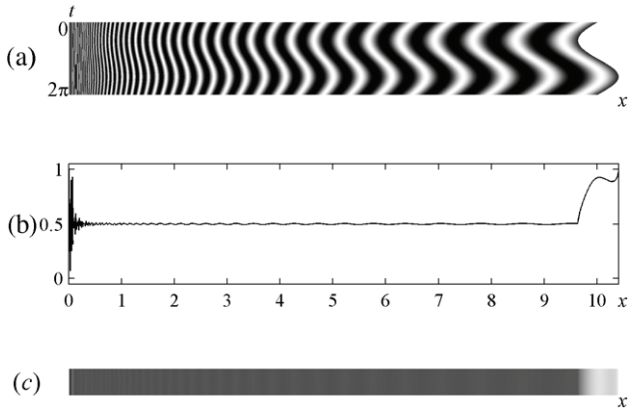

Figure 5. The oscillation of the variable pitch deformable moiré grating in time. One period of oscillation is illustrated in (a); time-averaged grayscale levels and the optical interpretation of the time-averaged image are shown in (b) and (c) respectively.

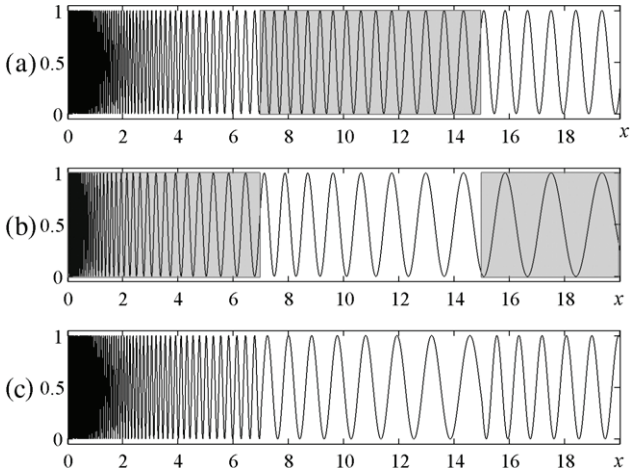

Figure 6. The formation of the composite moiré grating: non-shaded parts from (a) and (b) are copied into (c); the phase regularization algorithm is employed at the boundaries.

figure 5(b) does not show a fully developed time-averaged moiré fringe—that can be explained by the composite structure of the moiré grating. Nevertheless, the deviations from 0.5 are rather small—the naked eye cannot perceive any fluctuations in the optical representation of the time-averaged image in figure 5(c).

4. Dynamic visual cryptography based on a variable pitch deformable moiré grating

The formation of one row of pixels in the cover image is illustrated in a schematic diagram in figure 6. Let us assume that the secret image occupies the central part of the row ($7 \leq x \leq 15$) and the background image must be formed elsewhere (at $0 \leq x < 7$ and $15 < x \leq 20$). Also, let us assume that the background image is constructed using a moiré grating with the variable pitch $\lambda_0 = 0.05x$ (figure 6(a)) and a secret image with the variable pitch $\lambda_1 = 0.1x$ (figure 6(b)). Note that such a large difference between λ_0 and λ_1 in figure 6 is selected only for illustrative purposes. The first and the third parts of

Figure 7. The secret image.

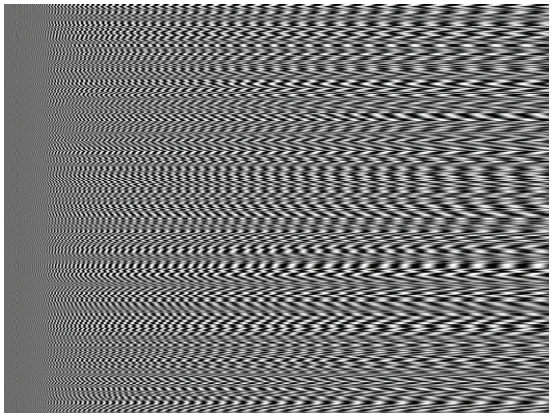

Figure 8. The secret image embedded into the cover image.

figure 6(a) are plotted on a white background—these parts are copied and pasted into the composite moiré grating shown in figure 6(c). Analogously, the central part (corresponding to the location of the secret image) is copied from figure 6(b) and pasted into figure 6(c). In fact, such a pasting procedure is not trivial—we use the phase regularization algorithm in order to equalize the phases of the composite moiré grating at the points of intersection between different gratings (which allows phase jumps to be avoided in the composite grating).

We will illustrate the applicability of variable pitch deformable moiré gratings for dynamic visual cryptography applications by the following computational example. Let us assume that the secret image is represented by the dichotomous non-convex shape shown in figure 7. We use a $\lambda_0 = 0.05x$ variable pitch for the background and a $\lambda_1 = 0.06x$ variable pitch for the secret image. A stochastic initial phase distribution [17] is employed for all rows of pixels in order to encode the cover image (figure 8). Note that moiré gratings in every row of pixels are continuous functions. The stochastic initial phase algorithm does not destroy the structure of the moiré grating in every row. Moreover, it does not alter the boundary between the background and the secret image. But it is impossible to see what secret picture is encoded into the static cover image by the naked eye.

The visual decoding of the cover image can be executed by employing deformable oscillations of the cover image according to the motion law described by (5). In other words,

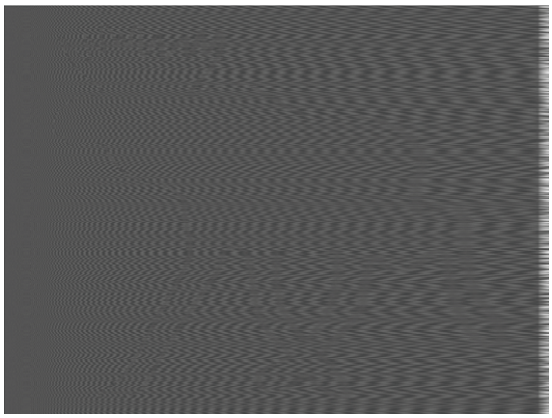

Figure 9. The time-averaged image at $A = 0.021$ does not leak the secret.

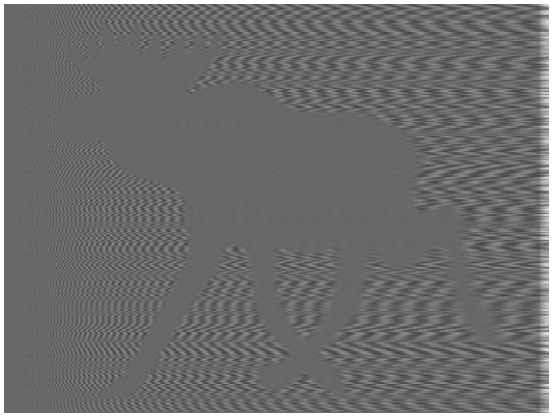

Figure 10. The time-averaged image at $A = 0.019$ does reveal the secret image.

the left side of the cover image must be motionlessly fixed; the right side of the deformable structure should be oscillated according to (5).

The secret image embedded into the cover image is leaked in the time-averaged image when the parameters of the oscillations satisfy relationship (18). It is impossible to see the secret image in figure 9—the amplitude $A = 0.021$ does not permit the formation of well-developed time-averaged moiré fringes. But the appropriate selection of the amplitude ($A = 0.019$) enables an effective visual decryption of the secret (figure 10). The visual quality of the leaked secret in figure 10 can be enhanced by employing the contrast enhancement techniques described in [20]—the decoded secret image is clearly visible in figure 11. The contrast enhancement techniques presented in [20] also serve as an optical criterion for the identification of moiré fringes in the time-averaged image—all regions occupied by time-averaged fringes are mapped into the black zones.

The formation of the secret image can be illustrated by setting different exposure times (fully developed time-averaged moiré fringes leak the secret image at the full period of oscillation in figure 10). One quarter, one half and three quarters of the period yield non-fully developed moiré fringes, which are illustrated in figure 12.

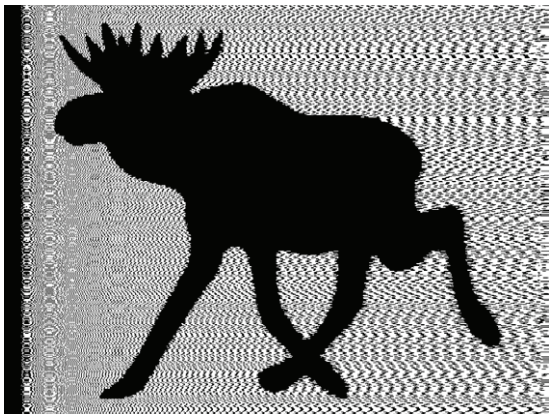

Figure 11. The contrast enhancement of the time-averaged image (figure 10).

The limit of the resolution of the proposed visual cryptography scheme is another important feature characterizing the applicability of this technique. All graphical primitives of the secret image are embedded into the stochastic moiré grating of the cover image. Therefore, the size of the smallest manageable detail of the secret image is directly related to pitch of the moiré grating. Thus, instead of measuring the size of the details in pixels or millimeters, we compare the size of the embedded object to the pitch of the moiré grating.

Let us assume that a square object represents the secret image and is embedded into the cover image. Also, it is assumed that the variation of the pitch of the moiré grating along the x-axis is slow—the pitch of the moiré grating is set to be constant (figure 13). Four computational experiments are used to illustrate the decryption of the secret image—when the size of the square is equal to $\frac{\lambda}{2}$ by $\frac{\lambda}{2}$ (figure 13(a)); λ by λ (figure 13(b)); $\frac{3\lambda}{2}$ by $\frac{3\lambda}{2}$ (figure 13(c)) and 2λ by 2λ (figure 13(d)). The amplitude of oscillation is set to $a = \frac{2\pi}{\lambda} r_1$, which guarantees the formation of the time-averaged moiré fringe inside the square. Every part of figure 13 represents two digital images—the time-averaged image of the cover image (on the left) and the contrast enhanced time-averaged image (on the right).

It is clear that the practical application of the proposed scheme requires that the smallest component of the secret image must occupy an area whose size is not less than a single pitch of the moiré grating (figure 13(b)).

5. Concluding remarks

The proposed image hiding technique leaks the secret when the cover image is deformed according to a predetermined periodic law of motion. No image splitting and no superposition of shares is required for decoding of the secret image, as all the information (the secret and the background) is stored in a single cover image. Moreover, the secret image can be observed by the naked eye only when the cover image performs predetermined oscillations.

We performed computational simulations for the illustration of optical effects. Building an experimental optical model is a more demanding task as compared with the DVC scheme

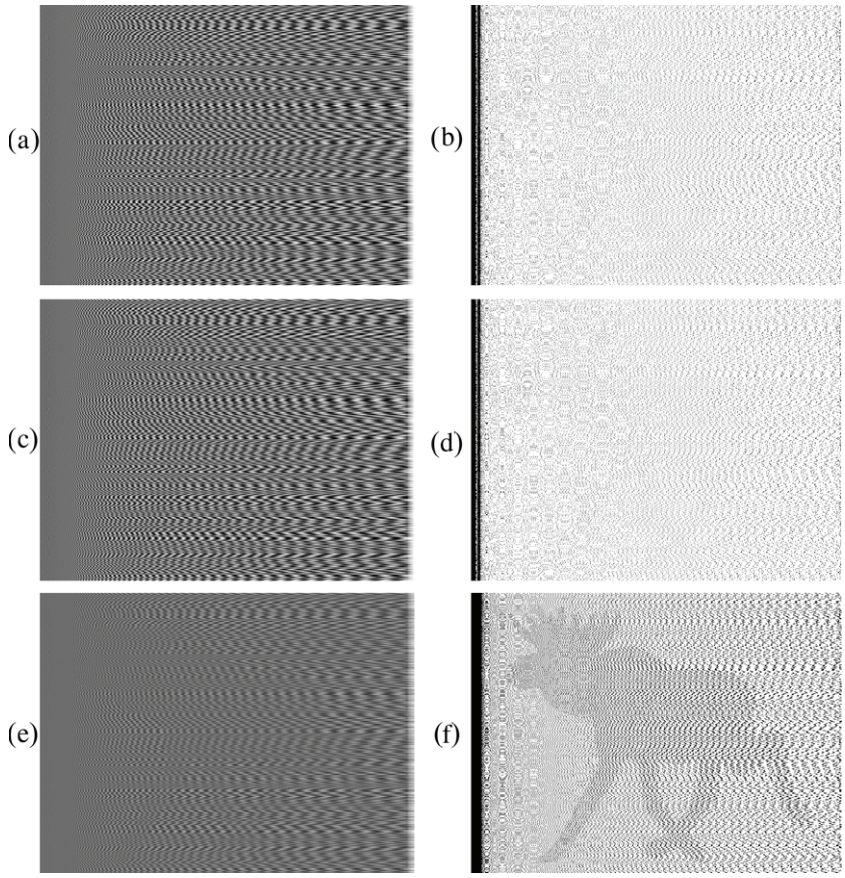

Figure 12. The formation of the secret image as the exposure time varies from one quarter of the period (a); half of the period (c); three quarters of the period (e) and the full period (figure 10). Contrast enhanced time-averaged images are shown in parts (b), (d) and (f) respectively.

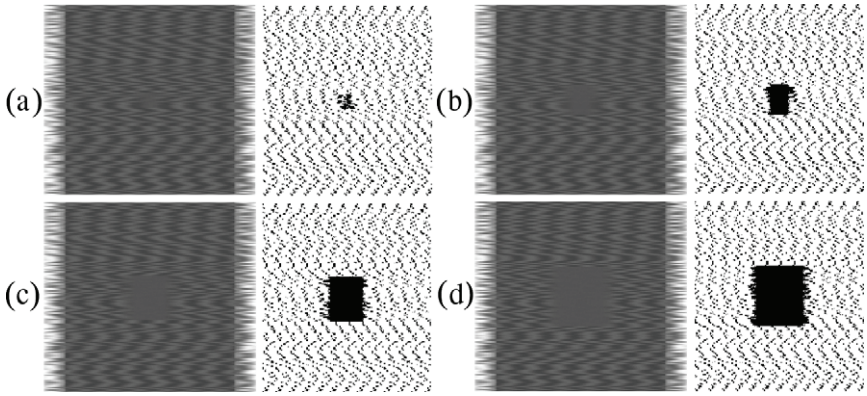

Figure 13. A schematic illustration of the minimum size of the secret image embedded into the cover moiré grating: the size of the square object is $\frac{\lambda}{2}$ by $\frac{\lambda}{2}$ (a); λ by λ (b); $\frac{3\lambda}{2}$ by $\frac{3\lambda}{2}$ (c) and 2λ by 2λ (d). Time-averaged images of the cover image are shown on the left; contrast enhanced time-averaged images are shown on the right.

based on non-deformable gratings. The main difference in the proposed image hiding scheme from already developed image hiding techniques based on oscillating cover images [17, 19] is in the type of oscillations. The secret image will not be leaked if the cover image (constructed using the proposed technique) oscillates as a non-deformable body in any direction, with any amplitude, and with any waveform. The necessary condition for visual decoding of the secret is the condition that the cover image must be deformed according to a predetermined periodic law of motion. Such an approach opens a completely new application area for optical control techniques in vibrating deformable structures. The development and practical implementation of such techniques is a definite objective of future research.

The cover image can be formed on the surface of a waveguide (or a piezoelectric actuator) in such a way that

the secret image is leaked when the waveguide oscillates with a predetermined eigenshape. Similar optical applications could be implemented in micro-opto-mechanical systems (MOEMS), where a stochastic cover moiré image could be formed on the surface of the cantilever. The secret image would be leaked when the tip of the cantilever oscillated at a predetermined amplitude (even though an optical microscope would be required to see the secret image). Moreover, dynamic visual cryptography based on deformable gratings can be used for the assessment of the human visual system (time-averaged moiré fringes are interpreted by visual cortex when eyes cannot follow the rapidly oscillating cover image) and the assessment of human fatigue (the frequency of oscillations at which the secret can be interpreted by the human brain can serve as a numerical measure of the fatigue).

Acknowledgment

Financial support form the Lithuanian Science Council under project No. MIP-100/2012 is acknowledged.

References

[1] Kobayashi A S 1993 *Handbook on Experimental Mechanics* 2nd edn (Bethel: SEM)
[2] Patorski K and Kujawinska M 1993 *Handbook of the Moiré Fringe Technique* (Amsterdam: Elsevier)
[3] Post D, Han B and Ifju P 1997 *High Sensitivity Moiré: Experimental Analysis for Mechanics and Materials* (Berlin: Springer)
[4] Dai F L and Wang Z Y 1999 Geometric micron moiré *Opt. Lasers Eng.* **31** 191–208
[5] Lebanon G and Bruckstein A M 2001 A variational approach to moiré pattern synthesis *J. Opt. Soc. Am.* A **18** 1371–81
[6] Lebanon G and Bruckstein A M 2001 On designing moiré patterns *Lect. Notes Comput. Sci.* **2134** 185–201
[7] Naor M and Shamir R 1994 Visual cryptography *Lect. Notes Comput. Sci.* **950** 1–12
[8] Hou Y C 2003 Visual cryptography for color images *Pattern Recognit.* **36** 1619–29
[9] Cimato S, De Prisco R and De Santis A 2007 Colored visual cryptography without color darkening *Theor. Comput. Sci.* **374** 261–76
[10] Cimato S, De Santis A, Ferrara A L and Masucci B 2005 Ideal contrast visual cryptography schemes with reversing *Inf. Process. Lett.* **93** 199–206
[11] Yang C N and Chung T H 2010 A general multi-secret visual cryptography scheme *Opt. Commun.* **283** 4949–62
[12] Wang R Z, Lan Y C, Lee Y K, Huang S Y, Shyu S J and Chia T L 2010 Incrementing visual cryptography using random grids *Opt. Commun.* **283** 4242–9
[13] Chen Y C, Tsai D S and Horng G 2012 A new authentication based cheating prevention scheme in NaorShamirs visual cryptography *J. Vis. Commun. Image Represent.* **23** 1225–33
[14] Liang C Y, Hung Y Y, Durelli A J and Hovanesian J D 1979 Time averaged moiré method for in-plane vibration analysis *J. Sound Vib.* **62** 267–75
[15] Lin C J and Chiang F P 1982 Time-average in-plane moiré method for the analysis of nonsinusoidal cyclic loading *Exp. Mech.* **22** 64–8
[16] Ragulskis M and Navickas Z 2009 Time average moiré—back to the basics *Exp. Mech.* **49** 439–50
[17] Ragulskis M and Aleksa A 2009 Image hiding based on time-averaging moiré *Opt. Commun.* **282** 2752–9
[18] Petrauskiene V, Aleksa A, Fedaravicius A and Ragulskis M 2012 Dynamic visual cryptography for optical control of vibration generation equipment *Opt. Lasers Eng.* **50** 869–76
[19] Ragulskis M, Aleksa A and Navickas Z 2009 Image hiding based on time-averaged fringes produced by non-harmonic oscillations *J. Opt. A: Pure Appl. Opt.* **11** 125411
[20] Ragulskis M, Aleksa A and Maskeliunas R 2009 Contrast enhancement of time-averaged fringes based on moving average mapping functions *Opt. Lasers Eng.* **47** 768–73